

CrossMark
click for updatesCite this: *Chem. Sci.*, 2016, 7, 1988

Origins of unique gold-catalysed chemo- and site-selective C–H functionalization of phenols with diazo compounds†

Yuan Liu,^{‡,ab} Zhunzhun Yu,^{‡,a} John Zenghui Zhang,^b Lu Liu,^{*a} Fei Xia^{*ab}
and Junliang Zhang^{*a}

In past decade, gold revealed more and more unique properties in carbene chemistry. It was disclosed in our recent communication (*J. Am. Chem. Soc.* 2014, **136**, 6904) that gold carbenes have unprecedented chemo- and site-selectivity and ligand effect toward the functionalization of C–H bonds in phenols. In this full article, we report a comprehensively combined theoretical and experimental study on the mechanism of the insertion of gold carbenes into C–H and O–H bonds in phenol. It significantly revealed that the ligands have an important effect on C–H insertion and the reaction proceeds through a pathway involving the formation of an enolate-like intermediate. Moreover, two water molecules serving as a proton shuttle are believed to be the key issue for achieving chemoselective C–H functionalization, which is strongly supported by the DFT calculations and control experiments. It is the first time that a clear explanation is given about the prominent catalysis of gold carbenes toward C–H functionalization based on a theoretical and experimental study.

Received 12th November 2015

Accepted 27th November 2015

DOI: 10.1039/c5sc04319k

www.rsc.org/chemicalscience

Introduction

Phenols are not only frequently found in natural products and pharmaceuticals, but are also powerful versatile platforms in organic synthesis.¹ Thus, the catalytic functionalization of phenols in a chemo- and site-selective manner is the most encompassing issue in organic chemistry.² In this context, the transition-metal-promoted decomposition of diazo compounds to generate metal carbenes has broad applications³ in the direct site-selective functionalization of phenols. In most cases, O–H insertion takes place catalysed by a series of transition-metal catalysts such as copper, palladium, iron, and rhodium complexes.⁴ In contrast, very recently, we and Shi independently found the unprecedented C(sp²)-H bond functionalization of phenols with α -diazoesters,⁵ furnishing *para*-substituted phenols **Pro-c8** via *para* C–H functionalization rather than the O–H insertion product **Pro-o8**. Meanwhile, the chemoselectivity is heavily dependent on the nature of the ligand of the gold

catalyst⁶ (Table 1). Although Nakamura and Pérez *etc.*⁷ have theoretically studied the mechanism of C(sp³)-H insertion with carbenes, and Shi and co-workers^{5b} analysed the electronic structures of gold carbenes by using Density Functional Theory (DFT) calculations, no comprehensive mechanistic insight on the overall pathways of aromatic C(sp²)-H insertion with carbenes has been provided so far. To further understand the origin of this unique behaviour of gold carbenes⁸ in site selective C–H functionalization of phenol, we decided to carry out DFT calculations and an experimental study to gain insights on the mechanism. Herein, we present a combined computational and experimental study to elucidate the origin of the ligand effect on the chemoselectivity. Furthermore, the trace amount of water in the reaction mixture serving as a proton shuttle is proposed to be the key to give rise to the product **Pro-c8** of C–H insertion, which is supported by our current DFT calculations and control experiments.

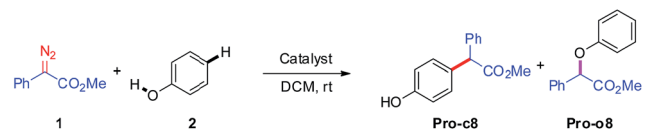
In a previous work on rhodium catalysed intramolecular aromatic C(sp²)-H insertion reactions, Padwa and Doyle assumed that the reactions were triggered by the electrophilic addition of the metallocarbene intermediate to the aromatic ring, then followed by a [1,2]-H migration step.⁹ Nevertheless, the reaction mechanisms for the prominent activity of gold carbenes toward C–H bonds still remain elusive. On the other hand, despite Yu and coworkers¹⁰ having performed the mechanistic study of the copper- and rhodium-catalysed O–H insertion of water with carbene using DFT calculations, the mechanism of gold-catalyzed O–H insertion has not yet been explored. In principle, there are three pivotal questions

^aShanghai Key Laboratory of Green Chemistry and Chemical Processes, School of Chemistry and Molecular Engineering, East China Normal University, 3663 N. Zhongshan Road, Shanghai 200062, China. E-mail: lliu@chem.ecnu.edu.cn; fxia@chem.ecnu.edu.cn; jlzhang@chem.ecnu.edu.cn

^bState Key Laboratory of Precision Spectroscopy, Institute of Theoretical and Computational Science & NYU-ECNU Center for Computational Chemistry at NYU Shanghai, 3663 Zhongshan Road North, Shanghai 200062, China

† Electronic supplementary information (ESI) available: Data for new compounds, experimental procedures and theoretical studies on mechanisms. See DOI: 10.1039/c5sc04319k

‡ These authors contributed equally to this work.

Table 1 C(sp²)-H bond functionalization of phenols with α -diazo-esters under various conditions


Entry	Catalyst (5 mol%)	Time	Pro-c8 ^a	Pro-o8 ^a
1 ^b	Cu(OTf) ₂	5 min	0	11
2 ^b	Cu(OTf)·toluene	5 min	0	9
3 ^b	[Pd(CH ₃ CN) ₂ Cl ₂]	12 h	0	33
4	Fe(OTf) ₂	12 h	NR	
5 ^c	FeCl ₂	12 h	0	0
6 ^b	[Rh ₂ (OAc) ₄]	5 min	0	36
7	Ph ₃ PAuSbF ₆	5 min	33	45
8	(PhO) ₃ PAuSbF ₆	5 min	82	0

^a NMR yield. ^b The conversion of **1** is 100% and the major product is dimer of **1**. ^c Trace amount of dimer from **1** was detected.

unsolved in this transformation: (1) is the mechanism of C(sp²)-H insertion with gold carbenes the same as that with other metals such as rhodium? (2) What is the origin of the ligand effect on the chemoselectivity? (3) Besides the ligand, any other factors affect the chemoselectivity?

Computational methods

All of the DFT calculations were carried out using the Gaussian 09 software package.¹¹ The geometric structure of the intermediates and transition states were optimized and located by using

the M06 functional,¹² since the M06 functional has been demonstrated to generate accurate results for organometallics especially in the description of noncovalent interactions. The LanL2dz basis set¹³ combined with the relativistic effective core potential for inner electrons and double zeta basis for covalent electrons was used to describe the heavy elements Au and P, and the 6-31G* basis set¹⁴ was used to describe the nonmetallic elements C, N, O and H. Frequency analyses were also performed based on the structures obtained in the gas phase to confirm that the intermediates are local minima and the transition states have only one imaginary frequency. Intrinsic reaction coordinate (IRC) calculations¹⁵ were performed to make sure that the crucial transition states connect the correct reactants and products. The solvent effect of CH₂Cl₂ was evaluated with single point calculations using the integral equation formalism model (IEFPCM)¹⁶ with the dielectric constant $\epsilon = 8.93$ based on the structures in the gas phase. All discussed energy values of intermediates and transition states throughout this paper are the Gibbs free energies in units of kcal mol⁻¹ that were calculated at the temperature of 298 K, including the corrections of solvation free energies from the IEFPCM model. The 3D images of the calculated structures were plotted using GaussView.¹⁷ More structural details of intermediates and transition states can be found in the ESI.†

Results and discussion

On the pathway of C-H functionalization catalysed by (PhO)₃PAuSbF₆

It has been widely accepted that metal catalysts could catalyse diazo compounds to release N₂ and form reactive Au-carbenes,

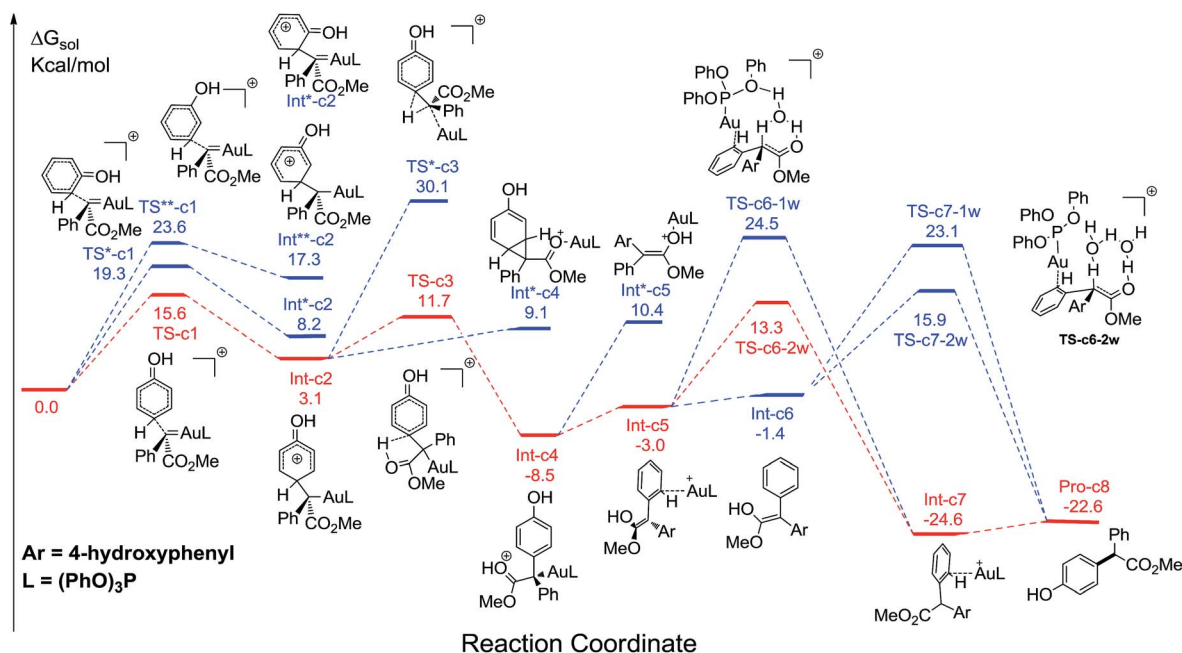


Fig. 1 The calculated free energy profiles ΔG and the corresponding structures of intermediates and transition states along different possible C-H insertion pathways catalyzed by (PhO)₃PAuSbF₆. The reasonable pathways are shown in red and other possible pathways are in blue. All values of free energies are relative to the gold carbene and phenol reactants and in the units of kcal mol⁻¹.

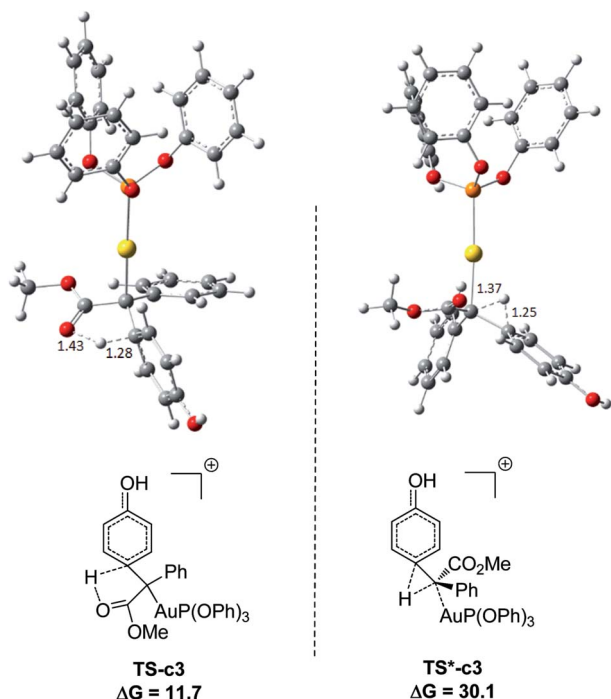


Fig. 2 Optimized structures of transition states TS-c3 and TS*-c3 corresponding to Fig. 1. The distances are in the units of angstroms and the values of free energies ΔG are in kcal mol⁻¹.

which were regarded as the precursors responsible for C-H bond insertion.^{5,8a-e} To account for the generation of crucial precursors preceding C-H insertion, we calculated the reaction pathways of α -diazoesters and metal catalysts AuL (L = (PhO)₃P and Ph₃P) in solution (Fig. S1 of ESI†). The calculated free energy profiles indicate that the generation of Au-carbene species is quite facile and drastically exothermic, with the low

barriers of 6.5 and 11.4 kcal mol⁻¹, respectively. Therefore, the gold carbenes and phenol are regarded as the reactants for the subsequent C-H bond insertion reactions and the sum of their free energies is set as the benchmark, with the value of 0.0 kcal mol⁻¹.

Fig. 1 displays the calculated free energy profiles for the C(sp²)-H functionalization of phenol with a gold carbene with (PhO)₃P as the ligand, where the structural details of intermediates and transition states are provided in the ESI.† The previous theoretical investigations on the C(sp³)-H insertion of rhodium, copper or silver carbenes, performed by Nakamura and Pérez, indicate that the first step of the reactions involves the formation of σ -bond complexes of carbenes and the C(sp³)-H bond.⁷ Recently, Pérez and coworkers suggested that the mechanism of aromatic C(sp²)-H bond insertion might be entirely different from that of aliphatic C(sp³)-H bond insertion.^{8c} In our DFT calculations, a transition state **TS-c1** with a barrier of 15.6 kcal mol⁻¹ is located for the addition of the gold carbene at the *para*-position of phenol. **TS-c1** represents the transition state of the direct C(sp²)-C(sp²) coupling of phenol and the gold carbene, leading to the final *para*-C-H insertion product **Int-c2**. Accordingly, the addition of the carbene at the *ortho* site of phenol gives rise to an intermediate **Int*-c2** with a higher energy (8.2 kcal mol⁻¹ vs. **Int-c2**'s 3.1 kcal mol⁻¹) via the transition state **TS*-c1** with 19.3 kcal mol⁻¹. It is not surprising to find that the *meta*-position of phenol is the most unfavourable site for addition with the gold carbene, which needs an activation energy barrier up to 23.6 kcal mol⁻¹. Such high activation barriers of **TS*-c1** and **TS**-c1** prevent the carbenes from adding at the *ortho*- and *meta*-positions of phenol. The current DFT results are consistent with our experimental observations that the addition at the *para*-sites of substituted phenols was the predominant even with bulky steric hindrance (*i.e.* 3,5-dimethyl phenol).^{5a} According to the previous calculations,¹⁰ the intermediate **Int-c2** may be

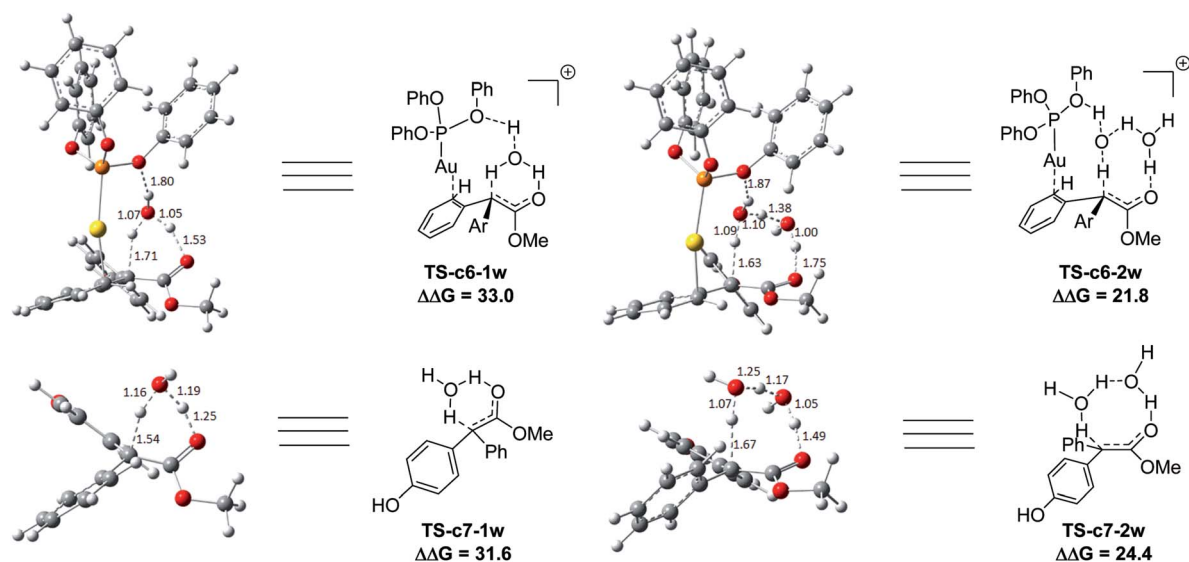
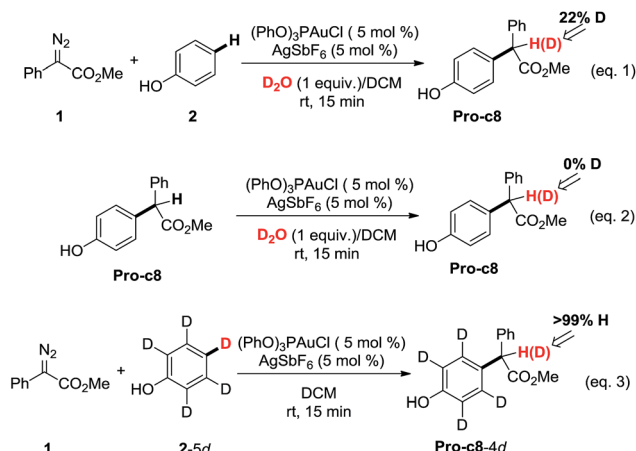


Fig. 3 The structures of TS-c6-1w, TS-c6-2w, TS-c7-1w and TS-c7-2w in the pathways of C-H functionalization of phenol catalysed by (PhO)₃PAuSbF₆. The values of the free energy barriers $\Delta\Delta G$ are in kcal mol⁻¹.





Scheme 1 Control experiments.

isomerized to the enolate *via* the mechanism of [1,3]-metal migration and yield a stable intermediate. However, it is found that such a stable intermediate hardly exists after the [1,3]-Au migration in **Int-c2**, since a kind of cyclopropanation product of the Büchner reaction is obtained, as shown by **Int*-c4**.¹⁸ Meanwhile, this process of [1,3]-Au migration seems to be energetically unfavorable, with the endothermicity of 9.1 kcal mol⁻¹ to give **Int*-c4**. Additionally, in order to examine whether the commonly accepted mechanism of direct [1,2]-H shift is feasible, we located the transition state **TS*-c3** with the corresponding structure displayed in Fig. 2. Our calculated results imply that **TS*-c3** has a considerable barrier of 30.1 kcal mol⁻¹, which could definitely rule out the mechanism of direct [1,2]-H shift in **Int-c2**. During the course of optimization, we happened to hypothesize that the carbonyl oxygen atom may intend to directly abstract the proton at the original *para*-site of

phenol *via* the five-membered transition state **TS-c3** in Fig. 2, to generate **Int-c4**. This process is quite facile according to the current calculations, merely with a small barrier of 8.6 kcal mol⁻¹. Also, **Int-c4** is more stable than **Int*-c4** by 17.6 kcal mol⁻¹. Subsequently, the intermediate **Int-c4** undergoes an unexpected isomerization to the enol **Int-c5** through [1,3]-migration of the metal complex (PhO)₃PAu⁺ to the phenyl ring rather than to **Int*-c5**.

Two possible pathways might exist between the enol **Int-c5** and the final product **Pro-c8**. One is the gold-associated pathway, where the proton transfers through **TS-c6-1w** or **TS-c6-2w** to yield the intermediate **Int-c7**. Then, the metal complex (PhO)₃PAu⁺ dissociates from **Int-c7** to yield **Pro-c8**. The other is the gold-free pathway, where the catalyst (PhO)₃PAu⁺ first dissociates from **Int-c5** to yield the gold-free **Int-c6** and then proton transfer occurs *via* **TS-c7-1w** or **TS-c7-2w** to yield **Pro-c8**. As far as the two pathways are concerned, the key question is: how does the proton transfer from the hydroxyl to the final carbon in the enol? In this work, we propose that the water in the solvent plays a crucial role in undertaking the remote proton shuttle. Based on this proposal, we located the one-water assisted transition states **TS-c6-1w** and **TS-c7-1w**, as well as the two-water assisted transition states **TS-c6-2w** and **TS-c7-2w** along the reaction pathways, with the corresponding activation energy barriers of the elementary steps displayed in Fig. 3. The DFT results indicate that **TS-c6-1w** and **TS-c7-1w** involving one water molecule has higher energy barriers than two-water assisted **TS-c6-2w** and **TS-c7-2w**. Fig. 3 shows that the carboxyl group in **TS-c6-1w** and **TS-c7-1w** has to distort from the planar structures to form hydrogen bonds with H₂O, but they still remain planar in **TS-c6-2w** and **TS-c7-2w**. The structural distortion in **TS-c6-1w** and **TS-c7-1w** might be the reason why they are in high energy states. Interestingly, it is found that the oxygen atoms in the ligand (PhO)₃P form hydrogen bonding

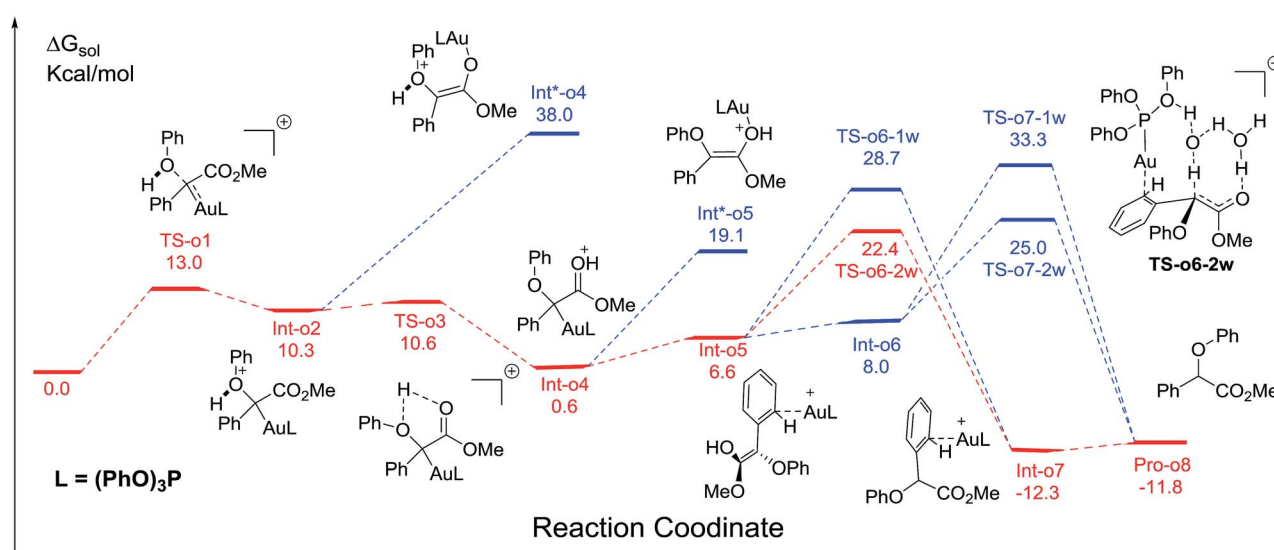


Fig. 4 The calculated free energy profiles ΔG and the corresponding structures of the intermediates and transition states along different possible O–H insertion pathways catalyzed by (PhO)₃PAuSbF₆. The reasonable pathway is shown in red and other possible pathways are in blue. All values of free energies are relative to the gold carbene and phenol reactants and in the units of kcal mol⁻¹.



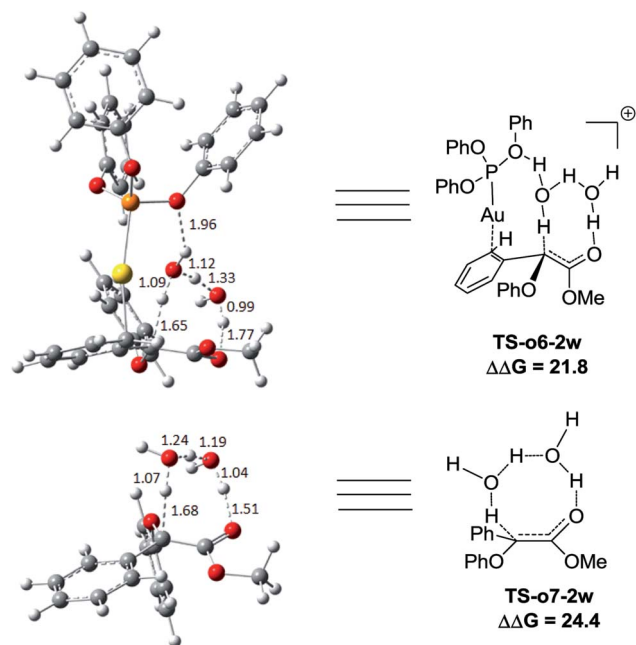


Fig. 5 The structures of TS-o6-2w and TS-o7-2w in the proposed O–H functionalization of phenols catalysed by $(\text{PhO})_3\text{PAuSbF}_6$. The distances are in the units of angstroms and the values of free energy barriers $\Delta\Delta G$ are in kcal mol^{-1} .

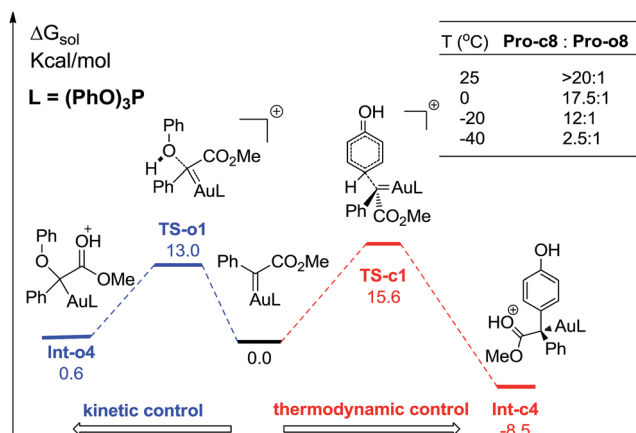


Fig. 6 The reaction temperature on the chemoselectivity and the competitive pathways for the formation of two key intermediates. All values of free energies are relative to the gold carbene and phenol reactants and in the units of kcal mol^{-1} .

Table 2 The calculated free energetic spans $\Delta\Delta G$ of hydrogen transfer through transition states (TSs) assisted by one water molecule and two water molecules in Fig. 6. The values of $\Delta\Delta G$ are in the units of kcal mol^{-1}

TSs	TS-c14-2w	TS-c15-2w	TS-o14-2w	TS-o15-2w
$\Delta\Delta G$	24.1	22.0	20.5	18.0

interactions with the shuttle water molecules in TS-c6-2w, while this effect does not exist in the other located transition state TS*-c6-2w (Fig. S2 in ESI†). The calculated distance between the

oxygen and hydrogen atoms in TS-c6-2w of Fig. 3 is 1.87 Å and the energy of the transition state is 2.2 kcal mol^{-1} lower than that of TS*-c6-2w, indicating a possible stabilization effect of the metal complex $(\text{PhO})_3\text{PAu}^+$ for the water chain in TS-c6-2w.

Control experiments were carried out in our lab (Scheme 1) to demonstrate the proposed mechanisms of gold carbene insertion into the C–H bond of phenol. When 1 equivalent of D_2O was added into the reaction system, product **Pro-o8** was deuterated with the percentage of 22% (eqn (1)). The relatively low deuterium ratio might be attributed to the existence of trace amount of H_2O ¹⁹ that could also undertake the function of proton transfer. Additionally, it is well known that the hydrogen in the OH group of phenol could readily exchange with the deuterium in D_2O , which leads to an increased H_2O or DOH amount in solution. If a great number of H_2O molecules participate in the process of the proton shuttle, the ratio of deuterated product **Pro-o8** will definitely decrease. We also considered the possibility whether the phenols can serve as the proton shuttle. However, the calculated energy barrier between the transition state structure TS-c6-2p (ESI†) and **Int-c5** for [1,3]-H shift is highly up to 36.1 kcal mol^{-1} , which implies that it hardly occurs. Eqn (2) manifests that the direct proton exchange of **Pro-o8** with D_2O is impossible under the reaction conditions. More importantly, eqn (3) demonstrates that the reaction of **1** and deuterated phenol 2-5d gives rise to the product **Pro-o8** without deuterium, which supports that direct [1,2]-H shift⁹ (TS*-c3) does indeed not occur in this case. The control experiments demonstrate that this kind of C–H bond insertion reactions governed by a gold carbene follows a novel mechanism involving a water assisting process, rather than previous commonly proposed direct [1,2]-H shift.^{5,8a,8c,9}

Proposed pathway of O–H insertion catalysed by $(\text{PhO})_3\text{PAuSbF}_6$

We next turn to address the question why the O–H insertion of phenol does not occur with $(\text{PhO})_3\text{PAuSbF}_6$ as the catalyst. In Fig. 4, the calculated results show that oxonium ylide²⁰ **Int-o2** formed through TS-o1 with a modest barrier. In the case of O–H bond insertion, a possible migration of complex LAu^+ to the carbonyl group in **Int-o2** is also taken into account, but the resulted structure **Int*-o4** is quite high in energy. The oxonium ylide **Int-o2** tends to isomerize to the more stable **Int-o4** via TS-o3. The migration of the gold catalyst to the phenyl group in **Int-o4** leads to the isomer **Int-o5**. It should be noted that **Int*-o5** is quite energetically unstable, with the gold complex attached to the oxygen atom in the hydroxyl group. Similarly to the mechanism of C–H insertion in Fig. 1, the rearrangements of **Int-o5** to **Pro-o8** pass through the gold-associated or gold-free pathways via the specific water-assisted transition states. We also locate the two-water assisted transition states TS-o6-2w for the gold-associated pathway and TS-o7-2w for the gold-free pathway, respectively (Fig. 5). The activation barrier of TS-o6-2w (15.8 kcal mol^{-1}) is relatively lower than that of TS-o7-2w (18.4 kcal mol^{-1}), indicating that the transformation of **Int-o5** to **Pro-o8** favours the gold-associated pathway via TS-o6-2w rather than TS-o7-2w.

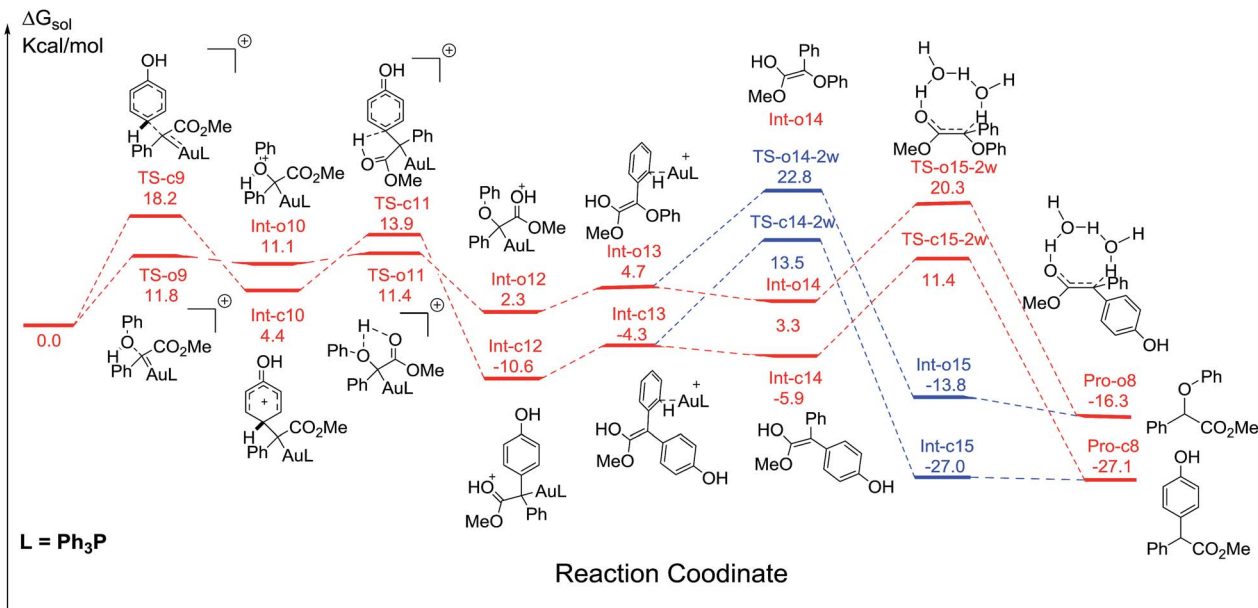


Fig. 7 The competitive pathways of C–H and O–H insertion catalyzed by $\text{Ph}_3\text{PAuSbF}_6$. The two reasonable pathways are shown in red and the other possible pathways in blue. All values of free energies are relative to the gold carbene and phenol reactants and in the units of kcal mol^{-1} .

Rationale of the chemoselectivity

Comparing these two competitive reaction pathways in Fig. 1 and 4, it is revealed that both rearrangements from **Int-c5** or **Int-o5** to the final products are the rate-determining steps in the overall pathways, with almost the same total barriers of $21.8 \text{ kcal mol}^{-1}$. Nevertheless, the DFT calculations reveal that the thermal stability of the intermediate of C–H insertion remarkably differs from that of O–H insertion. For example, the intermediate **Int-c4** is more stable than **Int-o4** by $9.1 \text{ kcal mol}^{-1}$, with an exothermic energy of $8.5 \text{ kcal mol}^{-1}$. As for the final products, the energy of **Pro-c8** is $10.8 \text{ kcal mol}^{-1}$ lower than that of the O–H insertion product **Pro-o8**. Besides, the endothermicity of **TS-c6-2w** is $13.3 \text{ kcal mol}^{-1}$, whereas the corresponding energy of **TS-o6-2w** is up to $22.4 \text{ kcal mol}^{-1}$, relative to the sum of the reactants. Such a large endothermicity of **TS-o6-2w** means that it is more difficult to pass through it to reach the product though collision in solution. The calculated reaction pathways in Fig. 1 and 4 reveal that the stability of intermediates plays an important role in chemoselectivity and accounts for the unique chemoselectivity toward C(sp²)-H insertion.

In order to further understand the chemoselectivity, the reactions of phenol with α -phenyldiazoester catalysed by $(\text{PhO})_3\text{PAuSbF}_6$ at different temperatures were also carried out. The ratios of **Pro-c8** : **Pro-o8** decreased from $>20 : 1$ to $2.5 : 1$ along with lowering the reaction temperature from rt to -40°C (Fig. 6; for details, see ESI†). These results indicated that the C–H functionalization process was more favored at high temperature than at low temperature. According to the free energy showed in Fig. 1 and 4, **Int-c4** and **Int-o4** should be the key intermediates for C–H functionalization and O–H insertion. As shown in Fig. 6, **Int-c4** was more stable via a higher barrier whilst **Int-o4** was more unstable via a lower barrier. That is, the

formation of **Int-c4** was the process of thermodynamic control, leading to C–H functionalization. In contrast, the generation of **Int-o4** underwent kinetic control, leading to O–H insertion. The control experiments at different temperatures and DFT calculations are in excellent agreement.

Two competitive pathways catalyzed by $\text{Ph}_3\text{PAuSbF}_6$

Additionally, the mechanisms of C–H and O–H insertions of phenol catalyzed by $\text{Ph}_3\text{PAuSbF}_6$ are also shown in Fig. 7, with the corresponding barriers listed in Table 2. On the one hand, compared to the corresponding pathways in Fig. 1 and 4, we found that the ligand Ph_3P has a remarkable electronic effect on the change of dynamics barriers of electrophilic addition to intermediates **Int-o12** and **Int-c12**. For C–H insertion, the addition barrier via **TS-c9** was enhanced to be $18.2 \text{ kcal mol}^{-1}$, $2.6 \text{ kcal mol}^{-1}$ higher than that of **TS-c1**. In contrast, the barrier of O–H insertion via **TS-o9** decreases from 13.0 to $11.8 \text{ kcal mol}^{-1}$. It is no doubt that the change of the barriers of addition is disadvantageous to C–H insertion but advantageous to O–H insertion. On the other hand, the calculated barrier of hydrogen transfer via **TS-o15-2w** in O–H insertion is $18.0 \text{ kcal mol}^{-1}$, relatively lower than the barrier of $22.0 \text{ kcal mol}^{-1}$ for C–H insertion. Therefore, the reaction of C–H insertion shown in Fig. 7 is significantly slowed down in comparison to the case when it is catalysed by $(\text{PhO})_3\text{PAuSbF}_6$ in Fig. 1. Product of C–H insertion is still more stable than the counterpart of O–H insertion in terms of thermodynamics according to the current DFT calculations. Considering both the dynamic and thermodynamic effects, the calculated pathways (Fig. 7) could account for the low chemoselectivity for **Pro-c8** and **Pro-o8** catalysed by $\text{Ph}_3\text{PAuSbF}_6$ that has been observed in our experiments (Table 1, entry 7).



Conclusions

In summary, the origins of the unique chemoselectivity of C–H bond functionalization of phenol with diazo compounds catalyzed by $(\text{PhO})_3\text{PAuSbF}_6$ are due to the high thermodynamic stability of intermediates and products, as well as the modest energy barrier of the rate-determining step. It is proposed for the first time that the reactions of gold carbenes with phenol pass through the specific pathways involving the formation of stable enols. The hydrogen transfers in the rearrangements from enol to final products follow a novel reaction pathway with two water molecules serving as a proton shuttle rather than the previous commonly proposed direct [1,2]-H shift. The DFT calculations also reveal that the oxygen atoms in the ligand $(\text{PhO})_3\text{P}$ play an important role in stabilizing the transition states of hydrogen transfer. The observed ligand effects of metal complexes on the reaction pathways are well rationalized based on the results of the present DFT calculations. The novel mechanistic insights delineated above will refine the model of gold catalyst in carbene chemistry and contribute to the future development of this field as well as the rational designing in chemo- and site-selective organic transformation.

Acknowledgements

Financial support by the 973 Program (2011CB808600), Shanghai Pujiang Program (14PJ1403100), National Natural Science Foundation of China (21572065, 21433004, 21473056, 21425205), Changjiang Scholars and Innovative Research Team in University (PCSIRT) is greatly appreciated. We acknowledge the support of the NYU-ECNU Center for Computational Chemistry at NYU Shanghai.

Notes and references

- 1 *Synthetic and Natural Phenols*, ed. J. H. P. Tyman, Elsevier, 1996.
- 2 For recent highlights, see: (a) D.-G. Yu, F. de Azambuja and F. Glorius, *Angew. Chem., Int. Ed.*, 2014, **53**, 7710; (b) P. MacLellan, *Nat. Chem.*, 2014, **6**, 375; for selected examples, see: (c) R. B. Bedford, S. J. Coles, M. B. Hursthouse and M. E. Limmert, *Angew. Chem., Int. Ed.*, 2003, **42**, 112; (d) R. B. Bedford and M. E. Limmert, *J. Org. Chem.*, 2003, **68**, 8669; (e) J. Luo, S. Preciado and I. Larrosa, *J. Am. Chem. Soc.*, 2014, **136**, 4109; (f) R. Zhu, J. Wei and Z.-J. Shi, *Chem. Sci.*, 2013, **4**, 3706; (g) Z. Huang, L. Jin, Y. Feng, P. Peng, H. Yi and A. Lei, *Angew. Chem., Int. Ed.*, 2013, **52**, 7151; (h) Z. Wu, F. Luo, S. Chen, Z. Li, H. Xiang and X. Zhou, *Chem. Commun.*, 2013, **49**, 7653; (i) H.-X. Dai, G. Li, X.-G. Zhang, A. F. Stepan and J.-Q. Yu, *J. Am. Chem. Soc.*, 2013, **135**, 7567; (j) A. Seoane, N. Casanova, N. Quiñones, J. L. Mascareñas and M. Gulías, *J. Am. Chem. Soc.*, 2014, **136**, 834; (k) Y. E. Lee, T. Cao, C. Torruellas and M. C. Kozłowski, *J. Am. Chem. Soc.*, 2014, **136**, 6782; (l) C. S. Sevov and J. F. Hartwig, *J. Am. Chem. Soc.*, 2013, **135**, 9303; (m) K. V. N. Esguerra, Y. Fall, L. Petitjean and J.-P. Lumb, *J. Am. Chem. Soc.*, 2014, **136**, 7662; (n) Y. Kuninobu, T. Matsuki and K. Takai, *J. Am. Chem. Soc.*, 2009, **131**, 9914; (o) C.-L. Ciana, R. J. Phipps, J. R. Brandt, F.-M. Meyer and M. J. Gaunt, *Angew. Chem., Int. Ed.*, 2011, **50**, 458.
- 3 For selected reviews, see: (a) *Modern Catalytic Methods for Organic Synthesis with Diazo Compounds: From Cyclopropanes to Ylides*, ed. M. P. Doyle, M. A. McKervey and T. Ye, Wiley-VCH, New York, 1998; (b) M. P. Doyle, R. Duffy, M. Ratnikov and L. Zhou, *Chem. Rev.*, 2010, **110**, 704; (c) H. M. L. Davies and Y.-J. Lian, *Acc. Chem. Res.*, 2012, **45**, 923; (d) H. M. L. Davies and D. Morton, *Chem. Soc. Rev.*, 2011, **40**, 1857; (e) M. M. Díaz-Requejo and P. J. Pérez, *Chem. Rev.*, 2008, **108**, 3379; (f) Z. Liu and J. Wang, *J. Org. Chem.*, 2013, **78**, 10024.
- 4 For reviews, see: (a) D. Gillingham and N. Fei, *Chem. Soc. Rev.*, 2013, **42**, 4918; (b) X. Guo and W. Hu, *Acc. Chem. Res.*, 2013, **46**, 2427; (c) S.-F. Zhu and Q.-L. Zhou, *Acc. Chem. Res.*, 2012, **45**, 1365; (d) D. J. Miller and C. J. Moody, *Tetrahedron*, 1995, **51**, 10811. For selected examples, see: (e) P. Yates, *J. Am. Chem. Soc.*, 1952, **74**, 5376; (f) Z. Zhu and J. H. Espenson, *J. Am. Chem. Soc.*, 1996, **118**, 9901; (g) Z. Qu, W. Shi and J. Wang, *J. Org. Chem.*, 2004, **69**, 217; (h) Z. Zhang, Y. Liu, L. Ling, Y. Li, Y. Dong, M. Gong, X. Zhao, Y. Zhang and J. Wang, *J. Am. Chem. Soc.*, 2011, **133**, 4330; (i) J. R. Sosa, A. A. Tadjarian and T. G. Minehan, *Org. Lett.*, 2008, **10**, 5091; (j) K. J. Kilpin, U. S. D. Paul, A.-L. Lee and J. D. Crowley, *Chem. Commun.*, 2011, **47**, 328; (k) R. A. Maurya, C. P. Park, J. H. Lee and D.-P. Kim, *Angew. Chem., Int. Ed.*, 2011, **50**, 5952; (l) T. Osako, D. Panichakul and Y. Uozumi, *Org. Lett.*, 2012, **14**, 194; (m) K. B. S. Magar and Y. R. Lee, *Org. Lett.*, 2013, **15**, 4288. For asymmetric version, see: (n) T. C. Maier and G. C. Fu, *J. Am. Chem. Soc.*, 2006, **128**, 4594; (o) C. Chen, S.-F. Zhu, B. Liu, L.-X. Wang and Q.-L. Zhou, *J. Am. Chem. Soc.*, 2007, **129**, 12616; (p) X.-L. Xie, S.-F. Zhu, J.-X. Guo, Y. Cai and Q.-L. Zhou, *Angew. Chem., Int. Ed.*, 2014, **53**, 2978.
- 5 (a) Z. Yu, B. Ma, M. Chen, H.-H. Wu, L. Liu and J. Zhang, *J. Am. Chem. Soc.*, 2014, **136**, 6904; (b) Y. Xi, Y. Su, Z. Yu, B. Dong, E. J. McClain, Y. Lan and X. Shi, *Angew. Chem., Int. Ed.*, 2014, **53**, 9817.
- 6 For selected recent accounts and general reviews, see: (a) A. Corma, A. Leyva-Perez and M. J. Sabater, *Chem. Rev.*, 2011, **111**, 1657; (b) C. Aubert, L. Fensterbank, P. Garcia, M. Malacria and A. Simonneau, *Chem. Rev.*, 2011, **111**, 1954; (c) N. Krause and C. Winter, *Chem. Rev.*, 2011, **111**, 1994; (d) M. Bandini, *Chem. Soc. Rev.*, 2011, **40**, 1358; (e) B.-L. Lu, L. Dai and M. Shi, *Chem. Soc. Rev.*, 2012, **41**, 3318; (f) D. Garayalde and C. Nevado, *ACS Catal.*, 2012, **2**, 1462; (g) Y.-W. Sun, Q. Xu and M. Shi, *Beilstein J. Org. Chem.*, 2013, **9**, 2224; (h) F. López and J. L. Mascareñas, *Beilstein J. Org. Chem.*, 2013, **9**, 2250; (i) G. Cera and M. Bandini, *Isr. J. Chem.*, 2013, **53**, 848; (j) W. Yang and A. S. K. Hashmi, *Chem. Soc. Rev.*, 2014, **43**, 2941; (k) F. López and J. Mascareñas, *Chem. Soc. Rev.*, 2014, **43**, 2904; (l) C. Obradors and A. M. Echavarren, *Acc. Chem. Res.*, 2014, **47**, 902; (m) A. S. K. Hashmi, *Acc. Chem. Res.*, 2014, **47**, 864; (n) L. Zhang, *Acc. Chem. Res.*, 2014, **47**, 877; (o) F. López



- and J. L. Mascareñas, *Beilstein J. Org. Chem.*, 2011, **7**, 1075; (p) D. Qian and J. Zhang, *Chem. Rec.*, 2014, **14**, 280; (q) D. Qian and J. Zhang, *Chem. Soc. Rev.*, 2015, **44**, 677.
- 7 (a) E. Nakamura, N. Yoshikai and M. Yamanaka, *J. Am. Chem. Soc.*, 2002, **124**, 7181; (b) A. A. C. Braga, F. Maseras, J. Urbano, A. Caballero, M. M. Díaz-Requejo and P. J. Pérez, *Organometallics*, 2006, **25**, 5292.
- 8 For gold-catalyzed carbene transfer from diazo compounds, see: (a) M. R. Frutos, T. R. Belderrain, P. de Frémont, N. M. Scott, S. P. Nolan, M. M. Díaz-Requejo and P. J. Pérez, *Angew. Chem., Int. Ed.*, 2005, **44**, 5284; (b) M. R. Frutos, P. de Frémont, S. P. Nolan, M. M. Díaz-Requejo and P. J. Pérez, *Organometallics*, 2006, **25**, 2237; (c) I. Rivilla, B. P. Gómez-Emeterio, M. R. Frutos, M. M. Díaz-Requejo and P. J. Pérez, *Organometallics*, 2011, **30**, 2855; (d) E. López, G. Lonzi and L. A. López, *Organometallics*, 2014, **33**, 5924; (e) J. Barluenga, G. Lonzi, M. Tomás and L. A. López, *Chem.-Eur. J.*, 2013, **19**, 1573; (f) J. F. Briones and H. M. L. Davies, *J. Am. Chem. Soc.*, 2012, **134**, 11916; (g) J. F. Briones and H. M. L. Davies, *J. Am. Chem. Soc.*, 2013, **135**, 13314; (h) Z.-Y. Cao, X. Wang, C. Tan, X.-L. Zhao, J. Zhou and K. Ding, *J. Am. Chem. Soc.*, 2013, **135**, 8197; (i) V. V. Pagar, A. M. Jadhav and R. S. Liu, *J. Am. Chem. Soc.*, 2011, **133**, 20728; (j) A. M. Jadhav, V. V. Pagar and R.-S. Liu, *Angew. Chem., Int. Ed.*, 2012, **51**, 11809; (k) S. K. Pawar, C.-D. Wang, S. Bhunia, A. M. Jadhav and R.-S. Liu, *Angew. Chem., Int. Ed.*, 2013, **52**, 7559; (l) D. Zhang, G. Xu, D. Ding, C. Zhu, J. Li and J. Sun, *Angew. Chem., Int. Ed.*, 2014, **53**, 11070; (m) G. Xu, C. Zhu, W. Gu, J. Li and J. Sun, *Angew. Chem., Int. Ed.*, 2015, **54**, 883; (n) Y. Zhou, B. G. Trewyn, R. J. Angelici and L. K. Woo, *J. Am. Chem. Soc.*, 2009, **131**, 11734; (o) G. Lonzi and L. A. López, *Adv. Synth. Catal.*, 2013, **355**, 1948; (p) A. Prieto, M. R. Frutos, M. M. Díaz-Requejo, P. J. Pérez, P. Pérez-Galán, N. Delpont and A. M. Echavarren, *Tetrahedron*, 2009, **65**, 1790.
- 9 A. Padwa, D. J. Austin, A. T. Price, M. A. Semones, M. P. Doyle, M. N. Protopopova, W. R. Winchester and A. Tran, *J. Am. Chem. Soc.*, 1993, **115**, 8669.
- 10 Y. Liang, H. Zhou and Z.-X. Yu, *J. Am. Chem. Soc.*, 2009, **131**, 17783.
- 11 M. J. Frisch, G. W. Trucks, H. B. Schlegel, G. E. Scuseria, M. A. Robb, J. R. Cheeseman, G. Scalmani, V. Barone, B. Mennucci, G. A. Petersson, H. Nakatsuji, M. Caricato, X. Li, H. P. Hratchian, A. F. Izmaylov, J. Bloino, G. Zheng, J. L. Sonnenberg, M. Hada, M. Ehara, K. Toyota, R. Fukuda, J. Hasegawa, M. Ishida, T. Nakajima, Y. Honda, O. Kitao, H. Nakai, T. Vreven, J. A. Montgomery Jr, J. E. Peralta, F. Ogliaro, M. Bearpark, J. J. Heyd, E. Brothers, K. N. Kudin, V. N. Staroverov, R. Kobayashi, J. Normand, K. Raghavachari, A. Rendell, J. C. Burant, S. S. Iyengar, J. Tomasi, M. Cossi, N. Rega, J. M. Millam, M. Klene, J. E. Knox, J. B. Cross, V. Bakken, C. Adamo, J. Jaramillo, R. Gomperts, R. E. Stratmann, O. Yazyev, A. J. Austin, R. Cammi, C. Pomelli, J. W. Ochterski, R. L. Martin, K. Morokuma, V. G. Zakrzewski, G. A. Voth, P. Salvador, J. J. Dannenberg, S. Dapprich, A. D. Daniels, Ö. Farkas, J. B. Foresman, J. V. Ortiz, J. Cioslowski and D. J. Fox, *Gaussian 09, Revision B.01*, Gaussian, Inc., Wallingford CT, 2009.
- 12 (a) Y. Zhao and D. G. Truhlar, *Theor. Chem. Acc.*, 2008, **120**, 215; (b) Y. Zhao and D. G. Truhlar, *Acc. Chem. Res.*, 2008, **41**, 157.
- 13 (a) P. J. Hay and W. R. Wadt, *J. Chem. Phys.*, 1985, **82**, 299; (b) W. R. Wadt and P. J. Hay, *J. Chem. Phys.*, 1985, **82**, 284.
- 14 V. A. Rassolov, M. A. Ratner, J. A. Pople, P. C. Redfern and L. A. Curtiss, *J. Chem. Phys.*, 2001, **22**, 976.
- 15 K. Fukui, *Acc. Chem. Res.*, 1981, **14**, 363.
- 16 G. Scalmani and M. J. Frisch, *J. Chem. Phys.*, 2010, **132**, 114110.
- 17 R. Dennington, T. Keith and J. Millam, *GaussView, Version 5*, Semichem Inc., Shawnee Mission, KS, 2009.
- 18 In order to rule out the pathway *via* the Büchner reaction, more control experiments were also carried out in our lab. Please see Section 3 in the ESI† for more details.
- 19 Y. Xia, Y. Liang, Y. Chen, M. Wang, L. Jiao, F. Huang, S. Liu, Y. Li and Z.-X. Yu, *J. Am. Chem. Soc.*, 2007, **129**, 3470.
- 20 For a nice experiment example of O–H insertion *via* oxonium ylides, see: X. Zhang, H. Huang, X. Guo, X. Guan, L. Yang and W. Hu, *Angew. Chem., Int. Ed.*, 2008, **47**, 6647.

